numbers of genes with differential expression: cell cycle, 455; sporulation, 477; diauxic shift, 1,823; DNA damage, 1,718; and stress response, 866.

Trace-back algorithm

We used the following algorithm to define sections of the regulatory network used in each condition: (1) identify transcription factors as being 'present' in a condition if they have sufficiently high expression levels; (2) flag differentially expressed genes that appear in the regulatory network; (3) mark as 'active' the regulatory links between present transcription factors and differentially expressed genes; and (4) search for any other present transcription factors that are linked to a transcription factor with an already active link and make this connection active. The last step is repeated until no more links are made active. The same procedure identifies sub-networks that are active in particular phases of cell cycle and sporulation.

SANDY

This extends the methodology used by the TopNet software tool[27] and it evaluates each sub-network with the following: (1) standard statistics, including global measures of topology (k_{in}, k_{out}, l, and c)[6] and local motif occurrence (SIM, MIM and FFL)[4]; (2) follow-on statistics, including permanent and transient hub identification, interchange index (I) and counting the overlap in transcription factor usage (individual and pairs) across multiple conditions. (Hubs are transcription factors in the top 30%, by number of target genes, in at least one condition. The number of target genes is normalized to measure the relative influence of a transcription factor hub in a particular process.) In all cases, regulatory functions are obtained from the Saccharomyces Genome Database[28] and are current as of June 2004; and (3) a comparison of observations and random expectation by simulating sub-graphs that are similar in size to each sub-network, and calculating standard and follow-on statistics for them. Simulated sub-graphs sample the same number of differentially expressed genes and trace through the static network. We also tested the sensitivity of our observations to noise by randomly perturbing the static networks by 30% (random addition, deletion and replacement of interactions), tracing back from the original differentially expressed genes and then recalculating the statistics.

Received 15 January; accepted 24 June 2004; doi:10.1038/nature02782.

1. Jeong, H., Tombor, B., Albert, R., Oltvai, Z. N. & Barabasi, A. L. The large-scale organization of metabolic networks. *Nature* **407,** 651–654 (2000).
2. Guelzim, N., Bottani, S., Bourgine, P. & Kepes, F. Topological and causal structure of the yeast transcriptional regulatory network. *Nature Genet.* **31,** 60–63 (2002).
3. Milo, R. *et al.* Network motifs: simple building blocks of complex networks. *Science* **298,** 824–827 (2002).
4. Shen-Orr, S. S., Milo, R., Mangan, S. & Alon, U. Network motifs in the transcriptional regulation network of *Escherichia coli*. *Nature Genet.* **31,** 64–68 (2002).
5. Oltvai, Z. N. & Barabasi, A. L. Systems biology. Life's complexity pyramid. *Science* **298,** 763–764 (2002).
6. Barabasi, A. L. & Oltvai, Z. N. Network biology: understanding the cell's functional organization. *Nature Rev. Genet.* **5,** 101–113 (2004).
7. Milo, R. *et al.* Superfamilies of evolved and designed networks. *Science* **303,** 1538–1542 (2004).
8. Teichmann, S. A. & Babu, M. M. Gene regulatory network growth by duplication. *Nature Genet.* **36,** 492–496 (2004).
9. Svetlov, V. V. & Cooper, T. G. Review: compilation and characteristics of dedicated transcription factors in *Saccharomyces cerevisiae*. *Yeast* **11,** 1439–1484 (1995).
10. Horak, C. E. *et al.* Complex transcriptional circuitry at the G1/S transition in *Saccharomyces cerevisiae*. *Genes Dev.* **16,** 3017–3033 (2002).
11. Lee, T. I. *et al.* Transcriptional regulatory networks in *Saccharomyces cerevisiae*. *Science* **298,** 799–804 (2002).
12. DeRisi, J. L., Iyer, V. R. & Brown, P. O. Exploring the metabolic and genetic control of gene expression on a genomic scale. *Science* **278,** 680–686 (1997).
13. Cho, R. J. *et al.* A genome-wide transcriptional analysis of the mitotic cell cycle. *Mol. Cell* **2,** 65–73 (1998).
14. Chu, S. *et al.* The transcriptional program of sporulation in budding yeast. *Science* **282,** 699–705 (1998).
15. Gasch, A. P. *et al.* Genomic expression programs in the response of yeast cells to environmental changes. *Mol. Biol. Cell* **11,** 4241–4257 (2000).
16. Gasch, A. P. *et al.* Genomic expression responses to DNA-damaging agents and the regulatory role of the yeast ATR homolog Mec1p. *Mol. Biol. Cell* **12,** 2987–3003 (2001).
17. Odom, D. T. *et al.* Control of pancreas and liver gene expression by HNF transcription factors. *Science* **303,** 1378–1381 (2004).
18. Zeitlinger, J. *et al.* Program-specific distribution of a transcription factor dependent on partner transcription factor and MAPK signaling. *Cell* **113,** 395–404 (2003).
19. Watts, D. J. & Strogatz, S. H. Collective dynamics of 'small-world' networks. *Nature* **393,** 440–442 (1998).
20. Wagner, A. & Fell, D. A. The small world inside large metabolic networks. *Proc. R. Soc. Lond. B* **268,** 1803–1810 (2001).
21. Yu, H., Greenbaum, D., Xin Lu, H., Zhu, X. & Gerstein, M. Genomic analysis of essentiality within protein networks. *Trends Genet.* **20,** 227–231 (2004).
22. Martinez-Antonio, A. & Collado-Vides, J. Identifying global regulators in transcriptional regulatory networks in bacteria. *Curr. Opin. Microbiol.* **6,** 82–489 (2003).
23. Madan Babu, M. & Teichmann, S. A. Evolution of transcription factors and the gene regulatory network in *Escherichia coli*. *Nucleic Acids Res.* **31,** 1234–1244 (2003).
24. Pilpel, Y., Sudarsanam, P. & Church, G. M. Identifying regulatory networks by combinatorial analysis of promoter elements. *Nature Genet.* **29,** 153–159 (2001).
25. Simon, I. *et al.* Serial regulation of transcriptional regulators in the yeast cell cycle. *Cell* **106,** 697–708 (2001).
26. Ueda, H. R. *et al.* A transcription factor response element for gene expression during circadian night. *Nature* **418,** 534–539 (2002).
27. Yu, H., Zhu, X., Greenbaum, D., Karro, J. & Gerstein, M. TopNet: a tool for comparing biological sub-networks, correlating protein properties with topological statistics. *Nucleic Acids Res.* **32,** 328–337 (2004).
28. Christie, K. R. *et al.* Saccharomyces Genome Database (SGD) provides tools to identify and analyze sequences from *Saccharomyces cerevisiae* and related sequences from other organisms. *Nucleic Acids Res.* **32,** D311–D314 (2004).

Supplementary Information accompanies the paper on **www.nature.com/nature**.

Acknowledgements We thank P. Bertone, N. Domedel-Puig, E. Hovig, R. Jansen, K. Kleivi, G. Koentges, E. Koonin, B. Lenhard, A. Paccanaro, J. Rozowsky, J. Tegner, V. Trifonov, A. Todd, Y. Xia and H. Zao for comments on the paper. N.M.L. thanks the Anna Fuller Fund and the MRC LMB Visitor's Program. M.M.B. acknowledges financial support from the Cambridge Commonwealth Trust, Trinity College, Cambridge and the MRC LMB. M.G. is supported by the NSF and NIH.

Competing interests statement The authors declare that they have no competing financial interests.

Correspondence and requests for materials should be addressed to N.M.L., M.M.B., S.A.T. & M.G. (sandy@bioinfo.mbb.yale.edu).

Long-lasting self-inhibition of neocortical interneurons mediated by endocannabinoids

Alberto Bacci, John R. Huguenard & David A. Prince

Department of Neurology and Neurological Sciences, Stanford University School of Medicine, Stanford, California 94305, USA

Neocortical GABA-containing interneurons form complex functional networks responsible for feedforward and feedback inhibition and for the generation of cortical oscillations associated with several behavioural functions[1,2]. We previously reported that fast-spiking (FS), but not low-threshold-spiking (LTS), neocortical interneurons from rats generate a fast and precise self-inhibition mediated by inhibitory autaptic transmission[3]. Here we show that LTS cells possess a different form of self-inhibition. LTS, but not FS, interneurons undergo a prominent hyperpolarization mediated by an increased K^+-channel conductance. This self-induced inhibition lasts for many minutes, is dependent on an increase in intracellular $[Ca^{2+}]$ and is blocked by the cannabinoid receptor antagonist AM251, indicating that it is mediated by the autocrine release of endogenous cannabinoids. Endocannabinoid-mediated slow self-inhibition represents a powerful and long-lasting mechanism that alters the intrinsic excitability of LTS neurons, which selectively target the major site of excitatory connections onto pyramidal neurons; that is, their dendrites[4–7]. Thus, modulation of LTS networks after their sustained firing will lead to long-lasting changes of glutamate-mediated synaptic strength in pyramidal neurons, with consequences during normal and pathophysiological cortical network activities.

We obtained whole-cell recordings from fast-spiking and LTS interneurons in layer V of rat somatosensory neocortical slices. Cells were characterized electrophysiologically by their firing behaviours as described previously[8] (Fig. 1a, c, insets; see also Methods). All biocytin-filled LTS interneurons contained cholecystokinin (CCK) ($n = 7$; Supplementary Fig. S1), whereas FS cells were CCK-negative ($n = 4$; Supplementary Fig. S1), indicating that we sampled a homogeneous non-FS cell population.

Although LTS interneurons lack GABAergic autaptic transmission[3], we found a unique form of slow self-inhibition (SSI) in

42 of 43 LTS cells. Multiple trains of evoked action potentials (APs) (first and last train in series shown in Fig. 1b, d) were followed by a prominent hyperpolarization of resting membrane potential ($V_m = -60.5 \pm 0.6$ mV versus -69.2 ± 1.0 mV, before and 5 min after DC-induced firing; $n = 9$, $p \ll 0.0001$; Fig. 1a, e). The hyperpolarization was long-lasting (more than 35 min), occurred selectively in LTS cells (V_m in FS cells $= -65.7 \pm 1.9$ mV versus -65.6 ± 2.0 mV, before and 5 min after DC-induced firing; $n = 6$, $p > 0.9$; Figs 1c, e and 2d), and occurred in the presence of synaptic blockers (Methods). In a few LTS cells there was a partial recovery of V_m after 12–15 min (not shown). SSI onset was well fitted by an exponential function with a time constant of 43 s.

LTS cells tend to fire at relatively low frequencies (20–50 Hz) during network oscillations[9]. To test the dependence of SSI on firing frequency within and outside this range, we applied brief suprathreshold depolarizing current steps to evoke trains of 10-Hz or 50-Hz APs (Fig. 2a, b). Both 10-Hz and 50-Hz spike trains evoked prominent SSI, and responses were comparable in amplitude and duration (Fig. 2c, g), indicating that even relatively low-frequency firing can trigger self-inhibition in LTS interneurons. Neither 10-Hz (Fig. 2d, g) nor 50-Hz stimuli (not shown) induced SSI in FS interneurons. SSI was accompanied by a marked, long-lasting increase in membrane conductance (g_m) (2.9 ± 0.5 nS in control versus 4.6 ± 0.5 and 5.1 ± 0.8 nS after 3 and 10 min of SSI induction, respectively; $n = 9$, $p < 0.002$ in both cases; Figs 2c, e, h). FS interneurons showed no significant changes in g_m from

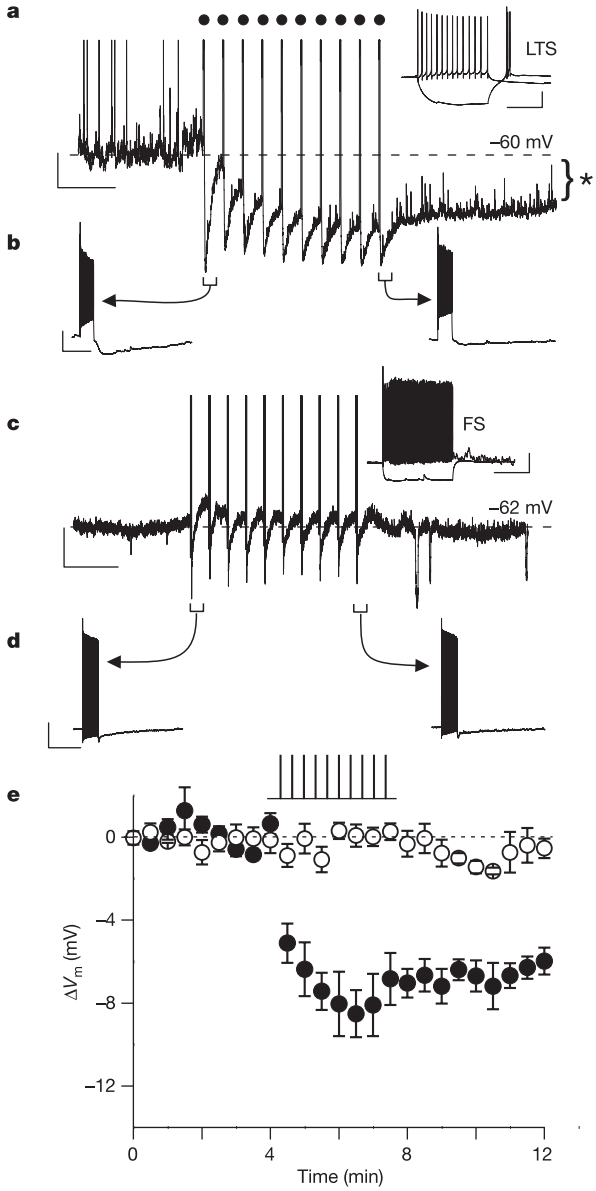

Figure 1 SSI occurs in LTS, not FS, neocortical interneurons. **a**, LTS interneuron responds to +600-pA current pulses (circles) with AP trains and long-lasting hyperpolarization (asterisk). Inset: LTS firing behaviour. **b**, First and last responses from **a**. **c**, **d**, As in **a** and **b**, but in a FS cell; SSI was not induced. Inset: FS firing behaviour. APs here and later have been truncated for display purposes. **d**, First and last responses from **c**. **e**, Changes in V_m (ΔV_m) in LTS cells (filled circles, $n = 9$) and FS cells (open circles, $n = 6$). Vertical lines indicate current pulses. Hyperpolarization was induced selectively in LTS cells. Scale bars, 1 min and 5 mV (**a**, **c**), 250 ms and 20 mV (insets), 2.5 s and 20 mV (**b**, **d**). Error bars indicate s.e.m.

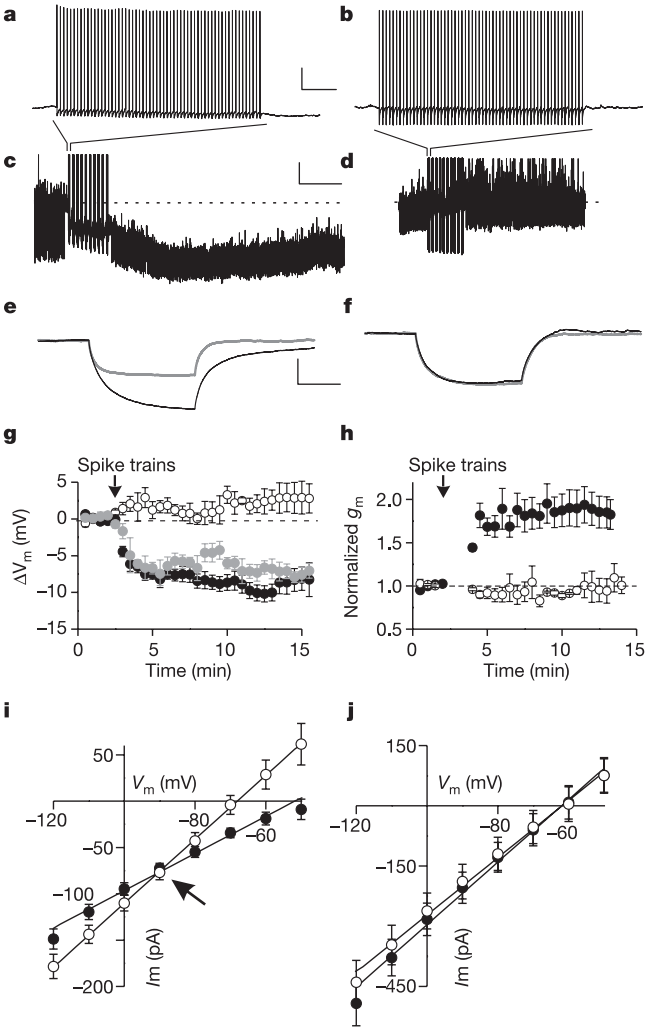

Figure 2 Low firing frequencies induce SSI, which reflects an increased membrane conductance. **a**, **b**, Brief depolarizing pulses reliably evoke LTS (**a**) and FS (**b**) spikes. **c**, **d**, Ten trains of 10-Hz APs elicited SSI in LTS (**c**) but not FS (**d**) cell. Negative deflections in **c**–**f** show conductance tests. **e**, **f**, Increased g_m (smaller responses) followed AP trains in LTS (**e**) but not FS (**f**) interneuron. Black traces, before trains; grey traces, after trains. **g**, Plot of ΔV_m against time during 50-Hz train stimulation (LTS (black filled circles), $p < 0.0001$, $n = 12$) and 10-Hz train stimulation (LTS (grey filled circles), $p < 0.01$, $n = 6$; FS (open circles), $p > 0.5$, $n = 4$). **h**, Normalized g_m time course in LTS (filled circles, $n = 9$) and FS (open circles, $n = 4$) interneurons. **i**, **j**, Current–voltage relationships in LTS (**i**, $n = 7$) and FS (**j**, $n = 6$) cells before trains (filled circles) and after trains (open circles). The arrow indicates the intersection of current–voltage plots in LTS cells. Scale bars, 20 mV and 1 s (**a**, **b**), 5 mV and 3 min (**c**, **d**), 5 mV and 100 ms (**e**, **f**). Error bars indicate s.e.m.

control when exposed to equivalent stimuli (3.8 ± 0.7 nS in control versus 3.6 ± 0.6 and 3.8 ± 0.8 nS after 3 and 10 min of SSI induction, respectively; $n = 4$, $p > 0.7$ in both cases; Fig. 2d, f, h).

The conductance underlying SSI was examined by using voltage-clamp recordings of membrane currents at different holding potentials. Current–voltage plots before and after stimulus trains intersected at about −90 mV, near the calculated K^+ equilibrium potential (Fig. 2i), but far from E_{Cl-} (about −16 mV), indicating activation of a K^+ conductance. Identical protocols applied to FS interneurons revealed no shifts in current–voltage relationships (Fig. 2j). Both the hyperpolarization and enhancement of g_m were reversed by the application of 0.1 mM Ba^{2+} after SSI induction (Supplementary Fig. S2), indicating that G-protein-coupled inwardly rectifying K^+ (GIRK) channels[10] are activated during SSI.

Sustained neuronal firing results in elevations of intracellular $[Ca^{2+}]$ that might contribute to SSI either by directly activating a Ca^{2+}-dependent membrane conductance or by enhancing the release of a transmitter/modulator that acts on autoreceptors of the stimulated cell[3,11]. We tested the role of increases in intracellular $[Ca^{2+}]$ in LTS self-inhibition by including the fast Ca^{2+} chelator BAPTA (10 mM) in the whole-cell pipette and assessing effects on SSI evoked as above. Intracellular BAPTA prevented the induction of SSI in LTS cells (Fig. 3a, c; $n = 6$), as did extracellular application of Cd^{2+} (200 μM) in the presence of control intracellular solution (Fig. 3b, c; $n = 6$), indicating that an elevation of $[Ca^{2+}]_i$ through voltage-dependent calcium channels triggers SSI in LTS cells. APs themselves were not required for SSI, because SSI could be induced in the presence of the Na^+-channel blocker tetrodotoxin (Supplementary Fig. S4).

We proposed that SSI might be induced by a Ca^{2+}-dependent release of a diffusible factor, acting on the same cells in an autocrine fashion. A prominent candidate would be an endocannabinoid, because the neuronal isoform of the G-protein-coupled cannabinoid receptor CB1 is selectively expressed by CCK-containing interneurons[12], and the LTS cells we recorded express this peptide (Supplementary Fig. S1). In addition, the synthesis of endocannabinoids is highly dependent on intracellular calcium elevations[12–14] that were presumably blocked along with SSI in our BAPTA and Cd^{2+} experiments. Moreover, activation of CB1 receptors leads to an increase of GIRK channel function[12,15].

To test the role of endocannabinoid receptors in LTS self-inhibition, we evoked spike trains as above, during local perfusion of the CB1 antagonist AM251 (ref. 16). AM251 (5 μM) blocked SSI induction in LTS cells (Fig. 4a, b; $n = 8$) as well as stimulus-induced

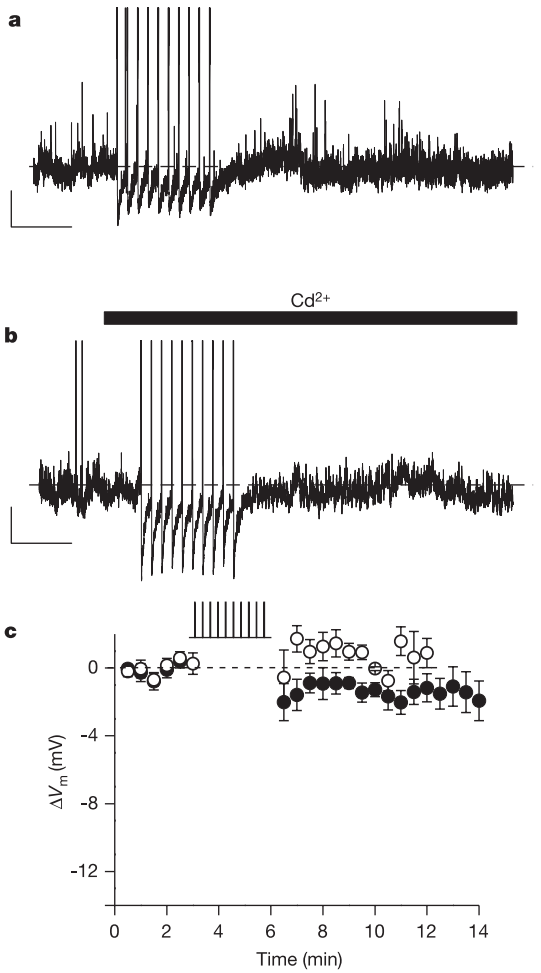

Figure 3 Intracellular increases in $[Ca^{2+}]$ through voltage-dependent Ca^{2+} channels are required for the induction of SSI in LTS cells. **a**, Response to SSI-inducing stimuli applied about 5 min into a whole-cell recording with intracellular BAPTA. **b**, Extracellular Cd^{2+} (200 μM) prevented SSI induction during a whole-cell recording, in the presence of intracellular EGTA. Scale bars, 5 mV and 2 min. **c**, V_m time course in LTS cells exposed to SSI stimuli in the presence of intracellular BAPTA (filled circles) or extracellular Cd^{2+} (open circles). Each treatment completely blocked SSI in all tested cells ($p > 0.4$ and $p > 0.1$ in BAPTA and Cd^{2+}, respectively; $n = 6$ in both cases). Error bars indicate s.e.m.

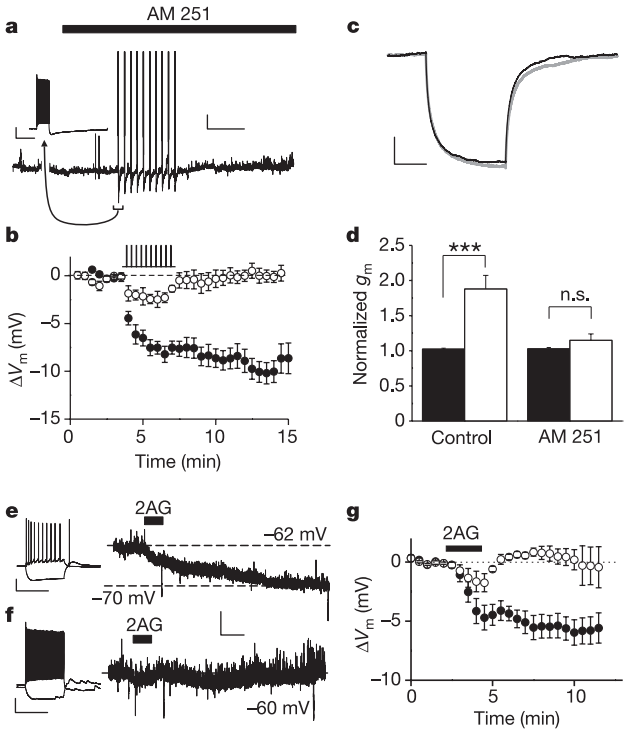

Figure 4 SSI is mediated by endocannabinoids. **a**, AM251 (5 μM) prevented SSI. Inset: response to first depolarizing pulse. **b**, ΔV_m time course in control (filled circles, $n = 12$) and AM251-treated (open circles, $n = 8$) cells; AM251 prevented SSI in all cells ($p > 0.7$, $n = 8$). Control data are from Fig. 2g. **c**, Conductance tests before (black trace) and after (grey trace) SSI-inducing stimuli in AM251. **d**, Normalized g_m in control and AM251-treated cells, before (filled columns) and after (open columns) spike trains. The increase in g_m (asterisks indicate $p < 0.002$; $n = 9$) was prevented by AM251 ($p > 0.1$; $n = 5$). **e**, **f**, Left: Current-clamp identification of LTS (**e**) and FS (**f**) cells. Right: responses to applications of 2AG (10 μM) in the same cells. **g**, Time course of the 2AG effect on V_m in LTS cells (filled circles, $p < 0.002$, $n = 7$) and FS cells (open circles, $p > 0.06$, $n = 6$). Scale bars, 5 mV and 2 min (**a**; **e** and **f** right), 20 mV and 500 ms (**a** inset; **e** and **f** left), 5 mV and 200 ms (**c**). Error bars indicate s.e.m.

increases in g_m (Fig. 4c, d). Moreover, AM251 applied after SSI induction partly reversed both the hyperpolarization and the change in g_m, indicating persistent CB1 receptor signalling during SSI expression (Supplementary Fig. S3). The relatively short (about 20-s) hyperpolarization that followed each evoked burst of APs in LTS and FS cells (Fig. 1a, c) was not related to SSI, because it was not altered by any of the above pharmacological manipulations (data not shown).

Finally, exogenous application of an endogenous cannabinoid, 2-arachidonylglycerol (2AG; 10 μM)[12], resulted in a robust hyperpolarization similar in amplitude and time course to that induced by spike trains (Fig. 4e, g). The 2-AG-mediated hyperpolarization was not elicited in FS cells (Fig. 4f, g; $n = 6$), indicating that this subtype of interneuron does not express GIRK-coupled somatodendritic CB1 receptors. This finding does not exclude the presence of such receptors on axonal terminals[12].

Here we show a novel form of self-inhibition in CCK-containing LTS cortical interneurons. SSI does not depend on glutamatergic and/or GABAergic neurotransmission, but rather on an activity-dependent long-lasting hyperpolarization due to the activation of a GIRK conductance, with the resultant depression of LTS interneuron excitability (see Supplementary Table 1 and Supplementary Fig. S3d). This plastic change in intrinsic LTS cell excitability is triggered by a Ca^{2+}-dependent autocrine action of endocannabinoids, which are probably synthesized by and targeted to the same neurons.

Recent studies have shown that endocannabinoids released by postsynaptic neurons mediate retrograde signalling at hippocampal and cerebellar synapses, underlying the transient (15–20 s) phenomena of depolarization-induced suppression of inhibition (DSI) and excitation (DSE)[16–18]. The proposed mechanism involves a negative modulation of presynaptic Ca^{2+} channels and transmitter release[12,16–18]. In hippocampus and neocortical layers II and III, DSI is due to retrograde effects of endocannabinoids on perisomatic terminals of basket cells containing CCK[2,19,20].

Our results differ from those involving DSI and DSE in several important respects. In neocortical layer V, repetitive firing of LTS interneurons at frequencies within their physiological range[9] induces a previously unknown endocannabinoid-mediated autocrine response—a persistent decrease in intrinsic excitability in the same LTS cells—that does not require retrograde signalling. In this model the highly lipophilic endocannabinoids, once synthesized, might affect nearby CB1 receptors by means of a localized intramembrane signalling mechanism[21]. The large Ba^{2+}-sensitive increases in g_m and the reversal potential of the underlying current indicate that, in contrast to the situation in DSI, CB1 receptors are present on neuronal somatodendritic membrane and are functionally coupled to K^+ channels. Recent data indicate that presynaptic K^+ channels might have a function in cerebellar DSI[22], and retrograde (but not autocrine) cannabinoid signalling also affects K^+ channels in cerebellar interneurons[23], although with kinetics that are shorter than SSI.

A long-lasting self-induced hyperpolarization similar to SSI might underlie two recently reported endocannabinoid-mediated effects in the hippocampus, namely a long-term depression of GABAergic transmission after tetanic stimulation[24], and persistent endocannabinoid signalling affecting the short-term plasticity of presynaptic GABA release from CB1-expressing interneurons[19].

Mechanisms underlying the long duration of SSI might include a sustained activation of CB1 receptors, as demonstrated by partial reversal of SSI with late AM251 applications (see Supplementary Fig. S3). Persistent endocannabinoid signalling could result from either altered metabolism through the catalytic enzyme fatty acid amide hydrolase, which is known to terminate endocannabinoid signalling[12,25], or to a relatively persistent change in CB1 activation state. A long-term downstream modification of the activated K^+ conductance, as might result from an alteration in channel phosphorylation[26], could contribute to SSI and might explain the incomplete effects of late AM251 application (Supplementary Fig. S3).

LTS and FS interneurons are connected through both electrical junctions and GABAergic synapses[27,28], forming two neocortical networks[9,28,29] with crucial roles in setting and maintaining cortical oscillations[2]. LTS interneuron axons target pyramidal cell dendrites[4–6], where most excitatory synapses are located[7]. The selective loss of LTS cell-evoked pyramidal dendritic inhibition during repetitive interneuronal discharge might therefore result in a prolonged enhancement of glutamatergic excitation onto cortical principal cells, altering their input–output relations and their participation in cortical network activities. Endocannabinoid-mediated, activity-dependent hyperpolarization in LTS cells might also have a crucial function in pyramidal cell disinhibition during epileptiform or other intense network activities known to be associated with the generation of high-frequency pyramidal cell and interneuronal firing[9,30]. Prolonged plastic changes in cortical signal processing mediated by SSI of LTS cells could be one important mechanism through which activation of CB1 receptors by the recreational drug marijuana gives rise to its psychotropic effects[12]. □

Methods

Preparation and electrophysiology of brain slices *in vitro*

Sprague–Dawley rats aged between postnatal day 13 (P13) and P21 were deeply anaesthetized with pentobarbital (50 mg kg^{-1}) and decapitated; brains were removed and immersed in cold (4 °C) 'cutting' solution containing (in mM): 234 sucrose, 11 glucose, 24 $NaHCO_3$, 2.5 KCl, 1.25 NaH_2PO_4, 10 $MgSO_4$ and 0.5 $CaCl_2$, gassed with 95% O_2/5% CO_2. Coronal slices (300 μm) were cut from somatosensory cortex (parietal area 1) with a vibratome and then incubated in oxygenated artificial cerebrospinal fluid containing (in mM): 126 NaCl, 26 $NaHCO_3$, 2.5 KCl, 1.25 NaH_2PO_4, 2 $MgSO_4$, 2 $CaCl_2$ and 10 glucose, pH 7.4, initially at 32 °C for 1 h, and subsequently at 23–25 °C, before being transferred to the recording chamber and maintained at 32 °C. Recordings were obtained from layer V interneurons identified visually, which were easily distinguished from pyramidal neurons by their lacking a large emerging apical dendrite. Interneuron subtypes were identified by single AP waveforms, firing frequency, degree of spike frequency accommodation and dynamic range[8], and by their GABAergic synaptic currents[8]. Depolarizing current pulses generated high-frequency, non-accommodating firing in FS cells. They lacked rebound spiking after hyperpolarizing current steps (Fig. 1c, inset) and had APs with prominent after-hyperpolarizations[8]. LTS cells generated a spike or a burst of spikes after hyperpolarizing current steps and had much lower firing frequencies and more spike frequency accommodation than FS cells[8] (Fig. 1a, inset). Intracellular labelling with biocytin was used to confirm the interneuronal morphology in some cells as reported previously[3,8] (data not shown, but see Supplementary Fig. S1). Experiments were performed in the whole-cell configuration of the patch-clamp technique. Electrodes (tip resistance 2–3 MΩ) were filled with an intracellular solution containing (in mM): potassium gluconate 70, KCl 70, NaCl 2, HEPES 10, EGTA 10, $MgCl_2$ 2; pH adjusted to 7.3 with KOH; 290 mOsm. In some experiments 10 mM BAPTA was substituted for 10 mM EGTA. Drugs were delivered with a local perfusion system composed of multiple fine tubes ending in a common outlet tube, positioned in proximity (about 250 μM) to the recorded neuron. Experiments were performed in the presence of the ionotropic glutamate receptor blockers 6,7-dinitroquinoxaline-2,3,dione (10 μM) and D,L-2-amino-5-phosphonovaleric acid (100 μM) in the bath and local perfusate. In some experiments the $GABA_A$ receptor blocker gabazine (10 μM) was included in the perfusate. Signals were amplified, with a Multiclamp 700A patch-clamp amplifier (Axon Instruments), sampled at 20 kHz and filtered at 10 kHz unless otherwise noted. A Digidata 1320 digitizer and PClamp9 (Axon Instruments) as well as locally generated software (J.R.H.) were used for data acquisition and analysis and for the generation of stimuli. The membrane conductance tests used involved measurements of responses to small current injections (−15 to 30 pA, 250 ms, 0.2 Hz). SSI-inducing stimuli consisted of ten trains of either 10-Hz or 50-Hz APs (60 APs per train), evoked every 20 s. Results are presented as means ± s.e.m. Unless otherwise noted, the paired Student's *t*-test was used to compare control data with those obtained in the same neurons after drug applications or 5–8 min after SSI-inducing stimuli. Differences were considered significant at $p < 0.05$.

Immunohistochemistry and histology

Biocytin (0.1–0.05%; Sigma) was included in the internal solution to fill neurons during electrophysiological recordings. Slices were subsequently fixed overnight in 4% paraformaldehyde in phosphate buffer (pH 7.4) at 4 °C, cryoprotected in 30% sucrose in 0.1 M phosphate buffer and sectioned (50 μm thickness) in a sliding microtome (MICROM International GmbH, Walldorf, Germany). Sections were treated twice in 50% ethanol for 10 min each time and blocked with 10% normal goat serum in PBS for 1 h, rinsed with PBS and incubated overnight with anti-CCK antibody (5 mg ml^{-1}, diluted 1:1,000 in PBS containing 0.5% Triton X-100). For CCK immunostaining we used a monoclonal antibody raised against CCK/gastrin (no. 28.2 monoclonal antibody) that was

kindly provided by G. Ohning (CURE/Digestive Diseases Research Center, Antibody/RIA Core, University of California, Los Angeles). Sections were rinsed twice in PBS and incubated for 2 h in the secondary antibody (goat anti-mouse coupled to fluorescein isothiocyanate, dilution 1:100; Molecular Probes), diluted in PBS plus 0.5% Triton X-100. Sections were rinsed in PBS and incubated for 1 h in Texas red Avidin D (diluted 1:1000; Vector Laboratories). Fluorescent biocytin-filled neurons and CCK immunoreactivity were then observed with a laser confocal microscope (Zeiss LSM510) and images were acquired.

Received 30 March; accepted 11 August 2004; doi:10.1038/nature02913.

1. McBain, C. J. & Fisahn, A. Interneurons unbound. *Nature Rev. Neurosci.* **2,** 11–23 (2001).
2. Freund, T. F. Interneuron diversity series: Rhythm and mood in perisomatic inhibition. *Trends Neurosci.* **26,** 489–495 (2003).
3. Bacci, A., Huguenard, J. R. & Prince, D. A. Functional autaptic neurotransmission in fast-spiking interneurons: a novel form of feedback inhibition in the neocortex. *J. Neurosci.* **23,** 859–866 (2003).
4. Thomson, A. M. & Deuchars, J. Synaptic interactions in neocortical local circuits: dual intracellular recordings *in vitro*. *Cereb. Cortex* **7,** 510–522 (1997).
5. Tamas, G., Buhl, E. H. & Somogyi, P. Fast IPSPs elicited via multiple synaptic release sites by different types of GABAergic neurone in the cat visual cortex. *J. Physiol. (Lond.)* **500,** 715–738 (1997).
6. Xiang, Z., Huguenard, J. R. & Prince, D. A. Synaptic inhibition of pyramidal cells evoked by different interneuronal subtypes in layer V of rat visual cortex. *J. Neurophysiol.* **88,** 740–750 (2002).
7. Williams, S. R. & Stuart, G. J. Dependence of EPSP efficacy on synapse location in neocortical pyramidal neurons. *Science* **295,** 1907–1910 (2002).
8. Bacci, A., Rudolph, U., Huguenard, J. R. & Prince, D. A. Major differences in inhibitory synaptic transmission onto two neocortical interneuron subclasses. *J. Neurosci.* **23,** 9664–9674 (2003).
9. Beierlein, M., Gibson, J. R. & Connors, B. W. A network of electrically coupled interneurons drives synchronized inhibition in neocortex. *Nature Neurosci.* **3,** 904–910 (2000).
10. Yamada, M., Inanobe, A. & Kurachi, Y. G protein regulation of potassium ion channels. *Pharmacol. Rev.* **50,** 723–760 (1998).
11. Pouzat, C. & Marty, A. Somatic recording of GABAergic autoreceptor current in cerebellar stellate and basket cells. *J. Neurosci.* **19,** 1675–1690 (1999).
12. Freund, T. F., Katona, I. & Piomelli, D. Role of endogenous cannabinoids in synaptic signaling. *Physiol. Rev.* **83,** 1017–1066 (2003).
13. Di Marzo, V. *et al.* Formation and inactivation of endogenous cannabinoid anandamide in central neurons. *Nature* **372,** 686–691 (1994).
14. Stella, N., Schweitzer, P. & Piomelli, D. A second endogenous cannabinoid that modulates long-term potentiation. *Nature* **388,** 773–778 (1997).
15. Mackie, K., Lai, Y., Westenbroek, R. & Mitchell, R. Cannabinoids activate an inwardly rectifying potassium conductance and inhibit Q-type calcium currents in AtT20 cells transfected with rat brain cannabinoid receptor. *J. Neurosci.* **15,** 6552–6561 (1995).
16. Kreitzer, A. C. & Regehr, W. G. Retrograde inhibition of presynaptic calcium influx by endogenous cannabinoids at excitatory synapses onto Purkinje cells. *Neuron* **29,** 717–727 (2001).
17. Wilson, R. I. & Nicoll, R. A. Endogenous cannabinoids mediate retrograde signalling at hippocampal synapses. *Nature* **410,** 588–592 (2001).
18. Ohno-Shosaku, T., Maejima, T. & Kano, M. Endogenous cannabinoids mediate retrograde signals from depolarized postsynaptic neurons to presynaptic terminals. *Neuron* **29,** 729–738 (2001).
19. Losonczy, A., Biro, A. A. & Nusser, Z. Persistently active cannabinoid receptors mute a subpopulation of hippocampal interneurons. *Proc. Natl Acad. Sci. USA* **101,** 1362–1367 (2004).
20. Trettel, J., Fortin, D. A. & Levine, E. S. Endocannabinoid signaling selectively targets perisomatic inhibitory inputs to pyramidal neurons in juvenile mouse neocortex. *J. Physiol. (Lond.)* **556,** 95–107 (2004).
21. Piomelli, D. The molecular logic of endocannabinoid signalling. *Nature Rev. Neurosci.* **4,** 873–884 (2003).
22. Diana, M. A. & Marty, A. Characterization of depolarization-induced suppression of inhibition using paired interneuron–Purkinje cell recordings. *J. Neurosci.* **23,** 5906–5918 (2003).
23. Kreitzer, A. C., Carter, A. G. & Regehr, W. G. Inhibition of interneuron firing extends the spread of endocannabinoid signaling in the cerebellum. *Neuron* **34,** 787–796 (2002).
24. Chevaleyre, V. & Castillo, P. E. Heterosynaptic LTD of hippocampal GABAergic synapses: a novel role of endocannabinoids in regulating excitability. *Neuron* **38,** 461–472 (2003).
25. Cravatt, B. F. *et al.* Supersensitivity to anandamide and enhanced endogenous cannabinoid signaling in mice lacking fatty acid amide hydrolase. *Proc. Natl Acad. Sci. USA* **98,** 9371–9376 (2001).
26. Wischmeyer, E., Doring, F. & Karschin, A. Acute suppression of inwardly rectifying Kir2.1 channels by direct tyrosine kinase phosphorylation. *J. Biol. Chem.* **273,** 34063–34068 (1998).
27. Galarreta, M. & Hestrin, S. A network of fast-spiking cells in the neocortex connected by electrical synapses. *Nature* **402,** 72–75 (1999).
28. Gibson, J. R., Beierlein, M. & Connors, B. W. Two networks of electrically coupled inhibitory neurons in neocortex. *Nature* **402,** 75–79 (1999).
29. Tamas, G., Somogyi, P. & Buhl, E. H. Differentially interconnected networks of GABAergic interneurons in the visual cortex of the cat. *J. Neurosci.* **18,** 4255–4270 (1998).
30. Grenier, F., Timofeev, I. & Steriade, M. Neocortical very fast oscillations (ripples, 80–200 Hz) during seizures: intracellular correlates. *J. Neurophysiol.* **89,** 841–852 (2003).

Supplementary Information accompanies the paper on **www.nature.com/nature**.

Acknowledgements We thank I. Parada for assistance during these experiments, and J. Krey for discussions. This work was supported by grants from the National Institute of Neurological Diseases and Stroke and the Pimley Research Fund.

Competing interests statement The authors declare that they have no competing financial interests.

Correspondence and requests for materials should be addressed to D.A.P. (daprince@stanford.edu).

Conserved mechanisms of glucose sensing and regulation by *Drosophila* corpora cardiaca cells

Seung K. Kim[1] **& Eric J. Rulifson**[2]

[1]*Departments of Developmental Biology and Medicine (Oncology Division), Stanford University School of Medicine, Beckman Center B300, Stanford, California 94305-5329, USA*
[2]*Department of Cell and Developmental Biology, University of Pennsylvania School of Medicine, 1214 BRB II/III, 421 Curie Boulevard, Philadelphia, Pennsylvania 19104-6058, USA*

Antagonistic activities of glucagon and insulin control metabolism in mammals, and disruption of this balance underlies diabetes pathogenesis. Insulin-producing cells (IPCs) in the brain of insects such as *Drosophila* also regulate serum glucose[1,2], but it remains unclear whether insulin is the sole hormonal regulator of glucose homeostasis and whether mechanisms of glucose-sensing and response in IPCs resemble those in pancreatic islets. Here we show, by targeted cell ablation, that *Drosophila* corpora cardiaca (CC) cells[3–5] of the ring gland are also essential for larval glucose homeostasis. Unlike IPCs, CC cells express *Drosophila* cognates of sulphonylurea receptor (Sur) and potassium channel (Ir), proteins that comprise ATP-sensitive potassium channels regulating hormone secretion by islets and other mammalian glucose-sensing cells[6–8]. They also produce adipokinetic hormone, a polypeptide with glucagon-like functions. Glucose regulation by CC cells is impaired by exposure to sulphonylureas, drugs that target the Sur subunit. Furthermore, ubiquitous expression of an *akh* transgene reverses the effect of CC ablation on serum glucose. Thus, *Drosophila* CC cells are crucial regulators of glucose homeostasis and they use glucose-sensing and response mechanisms similar to islet cells.

Insect corpora cardiaca (CC) are clusters of endocrine cells in the ring gland adjacent to the prothoracic gland and corpus allatum. A principal CC product is adipokinetic hormone (AKH), a polypeptide that mobilizes stored macromolecular energy reserves to sustain energy-consuming activities, such as crawling and flight. AKH is similar to mammalian glucagon[4]; like glucagon in pancreatic islet α-cells, AKH is synthesized as a pre-prohormone, processed, and stored in dense core vesicles[4,5]. Like mammalian glucagon activity in liver, AKH has been shown to bind a G-protein-coupled transmembrane receptor[9] and to increase lipolysis, glycogenolysis and production of trehalose in the insect fat body, a storage organ for lipid and glycogen[3,4].

Previous studies of AKH microinjection and ring gland transplantation in locusts and other insects[3,4] suggest that AKH is sufficient to increase haemolymph glucose concentrations, but have not yet shown a requirement for AKH in glucose homeostasis. To examine phenotypes resulting from CC cell ablation and AKH deficiency, we used a 1,000-base-pair DNA segment derived from sequences immediately 5′ of the *Drosophila akh* gene (see Supplementary Information) to drive the expression of the transcriptional trans-activator GAL4 (Fig. 1a) in CC cells. The *akh*–GAL4 construct, when crossed with a *UAS–mCD8GFP* (membrane-tethered green fluorescent protein, mGFP) reporter line, directed a GFP expression pattern that reflected endogenous *akh* expression in the ring gland corpora cardiaca of third-instar larvae (Fig. 1a, b). Using *in situ* hybridizations, we established that embryonic *akh* messenger RNA expression initiates in cells of the presumptive CC anlage (Fig. 2a) and that in later larval stages it is maintained only in CC cells (Figs 1a, b and 2b, c). To assess the role of the CC as an endocrine regulator of haemolymph glucose concentrations, we